



Innovation of Ultrafine Structured Alloy Coatings Having Superior Mechanical Properties and High Temperature Corrosion Resistance

X.Q. Ma, D.W. Gandy, and G.J. Frederick

(Submitted May 30, 2008; in revised form September 19, 2008)

High temperature protection requires full coating density, high adhesion, minor oxide inclusions, and preferably fine grains, which is not achievable in most thermal spray processes. High velocity oxygen fuel (HVOF) thermal spray process has been applied extensively for making such coatings with the highest density and adhesion strength, but the existence of not melted or partially melted particles are usually observed in the HVOF coatings because of relatively low flame temperature and short particle resident time in the process. This work has investigated the development of an innovative HVOF process using a liquid state suspension/slurry containing small alloy powders. The advantages of using small particles in a HVOF process include uniform coating, less defective microstructure, higher cohesion and adhesion, full density, lower internal stress, and higher deposition efficiency. Process investigations have proven the benefits of making alloy coatings with full density and high bond strength attributing to increased melting of the small particles and the very high kinetic energy of particles striking on the substrate. High temperature oxidation and hot corrosion tests at 800 °C have demonstrated that the alloy coatings made by novel LS-HVOF process have superior properties to conventional counterpart coatings in terms of oxidation rates and corrosion penetration depths.

Keywords boiler parts, corrosion of HVOF coatings, high temperature oxidation, HVOF spray parameters, HVOF microstructures, nanostructured materials, scratch or impact loading testing

1. Introduction

Of late, research and development of innovative thermal spray processes using liquid state feedstock, i.e., liquid precursors or suspensions, have attracted more attention and interest. It has been demonstrated that the new processes are very promising for making coatings with unique microstructures and superior properties (Ref 1-3).

So far, superfine-grained ceramic coatings have been manufactured mostly using the liquid-based plasma spray

This article is an invited paper selected from presentations at the 2008 International Thermal Spray Conference and has been expanded from the original presentation. It is simultaneously published in *Thermal Spray Crossing Borders, Proceedings of the 2008 International Thermal Spray Conference*, Maastricht, The Netherlands, June 2-4, 2008, Basil R. Marple, Margaret M. Hyland, Yuk-Chiu Lau, Chang-Jiu Li, Rogerio S. Lima, and Ghislain Montavon, Ed., ASM International, Materials Park, OH, 2008.

X.Q. Ma, Inframat Corporation, Farmington, CT; and D.W. Gandy and G.J. Frederick, Electric Power Research Institute, Charlotte, NC. Contact e-mail: xma@inframat.com.

processes. However, it is challenging to form a metallic coating by utilizing the same techniques. The challenges include at least: (1) to avoid severe oxidation of superfine metallic powders during spray; (2) to keep stable suspension of high density metallic powders; and (3) to determine spray window parameters for metallic powders typically having a wide range of size distribution. In a previous study, it was demonstrated that the technical obstacles could be overcome by hybridizing of HVOF spray technique and liquid suspension method, so-called LS-HVOF or SPS-HVOF for the first time (Ref 4).

Of the various thermal spray techniques available, high velocity oxygen fuel (HVOF) process gives the highest coating bond strength to substrate and the highest coating density, and thus has been proven to be more preferable for making the metallic coatings, as well as nanostructured ceramic coatings (Ref 5, 6). With innovative LS-HVOF process, further improvement in these HVOF merits can be achieved. This work will provide extensive investigation on the microstructures, mechanical properties, and especially corrosion performance of LS-HVOF-formed alloy coatings.

2. Experimental

2.1 Materials

An AISI 316L stainless steel was used as substrate in this study. The specimens have the dimensions of

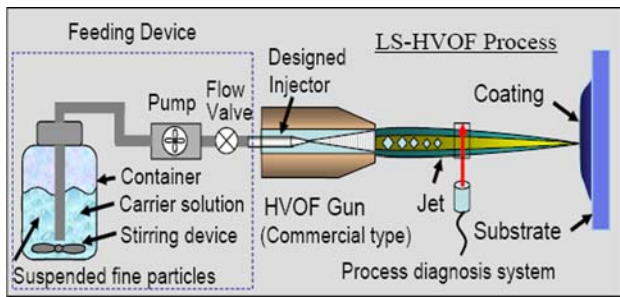


Fig. 1 Schematic of LS-HVOF process setup

$100 \times 100 \times 2.5 \text{ mm}^3$ for process trials, $60 \times 20 \times 2.5 \text{ mm}^3$ for mechanical property tests, and $10 \times 10 \times 2.5 \text{ mm}^3$ for oxidation and hot corrosion tests.

Two powders were purchased from a commercial vendor (Praxair, US). The powders have the identical nominal composition (wt.%) of Ni-14.55Cr-3.22B-4.7Si-4.78Fe, but different size distribution of $+16\text{-}42 \mu\text{m}$ for conventional HVOF use and of $-11 \mu\text{m}$ for innovative LS-HVOF use, respectively. Reagent grade chemicals were used to form liquid state suspensions (Ref 4).

2.2 LS-HVOF Setup

A Diamond Jet 2700 hybrid high velocity oxygen fuel (HVOF) spray system (Sulzer-Metco, NY, USA) equipped with a HVOF gun, a turntable, and a six-axis robot was used to spray the powder and suspension feedstock. Propylene was used as fuel, and routine surface preparation procedures were applied prior to the HVOF spraying. The spray parameters were optimized based on microstructural analyses and process diagnostic methods (Ref 4). In LP-HVOF process as shown in Fig. 1, the fine alloy powder was mixed well with the liquid solvent and was kept well suspended in a container. Then, the precursor was pumped to a liquid port and coaxially fed into the HVOF gun via a modified liquid injector. The flow of liquid precursor was controlled at a typical flow rate of 60-150 mL/min.

2.3 Test Methods

2.3.1 Microstructure Evaluation. Coating microstructures were evaluated according to a metallographic procedure, mainly on the cross sections using optical microscopy and electronic scanning microscopy (SEM). Coating grain structures were observed using transmission electronic microscopy (TEM). Coating porosity, unmelted particles, and coating/substrate interfaces were examined in these coatings. In addition, the oxygen contents in the coatings were analyzed using an oxygen-nitrogen analyzer (Leco TC-436) according to ASTM E1019-00.

2.3.2 Physical Property Tests. Microhardness (HVN) was measured on the cross sections of the coatings using a microhardness tester. Nanohardness and modulus was tested using a nano-indentation tester.

2.3.3 Mechanical Tests. Bending tests were carried out to determine coating cohesive strength/cracking resistance

and flexibility/ductility in accordance with the similar methods to ASTM B489-85 and ASTM D522. 90°-bending tests were conducted under both tensile and compressive loading modes. In 180° U-shape bending tests, a mandrel of 1" in diameter was used. The thickness of the coatings used in the bending tests is 150-180 μm .

Progressive load scratch test (PLST) was used to determine the critical loads corresponding to major coating damage failure and coating adhesion properties. This test corresponded to a load ramp applied to the indenter during defined displacement of the sample beneath it. In the test, 0.2 mm tip radius Rockwell diamond indenter tip was drawn across the coating with a loading rate of 300 N/min, start load of 0.9 N, and end load of 150 N. Using optical microscopy examination at 200 \times magnification, the critical loads (LC1, LC2, LC3, and LC4) were assessed.

2.3.4 Oxidation Tests. Short-term oxidation testing was used to determine the oxidation kinetics of the coatings in the early stages of oxide formation via TGA/DSC analyses. The rapid formation of protective oxides and low parabolic constant K_p represents better oxidation resistance. Long-term oxidation testing for 500 hours was conducted in a box furnace at 800 °C. Samples were put in a ceramic crucible, and weight changes were recorded every 50 h. The weight gain was plotted with time for each sample, and a parabolic constant was obtained by curve fitting method.

2.3.5 Hot Corrosion. Hot corrosion test was conducted in $\text{Na}_2\text{SO}_4 + 20\text{wt.}\% \text{NaCl}$ mixture salt at 800 °C. The salt was precoated evenly over the entire coating surfaces at a weight of 2-3 mg/cm^2 . The corrosion resistance of the coatings was measured by weight change and corrosion depth.

3. Results and Discussion

3.1 Microstructures

The typical microstructures and fractured morphologies of the coatings made by HVOF and LS-HVOF processes are shown in Fig. 2. In general, both coatings are well adherent to the substrates, quite dense, and crack-free. The LS-HVOF coating shows better microstructures with higher density and uniformity relative to conventional HVOF coating. The HVOF coating contains a high percentage of unmelted phase (as the arrows indicate in Fig. 2a and c) and at least 30 vol.%, and the average splat size is about 40 μm . In contrast, the LS-HVOF coating contains much less unmelts, and it is difficult to identify individual splats (Fig. 2b). As a result, the LS-HVOF coating is nearly full dense and is more uniform.

Oxygen content results are given in Table 1. The starting powders (with both fine and normal sizes) of NiCrBSi alloy contain about 0.06 wt.% oxygen. After HVOF processing, oxygen contents in the coatings were increased due to the "hot" nature of HVOF process and spraying in air. However, the oxygen content of 0.3% in the LS-HVOF coating is lower than that of 1% in the HVOF coating. It is believed that the use of organic

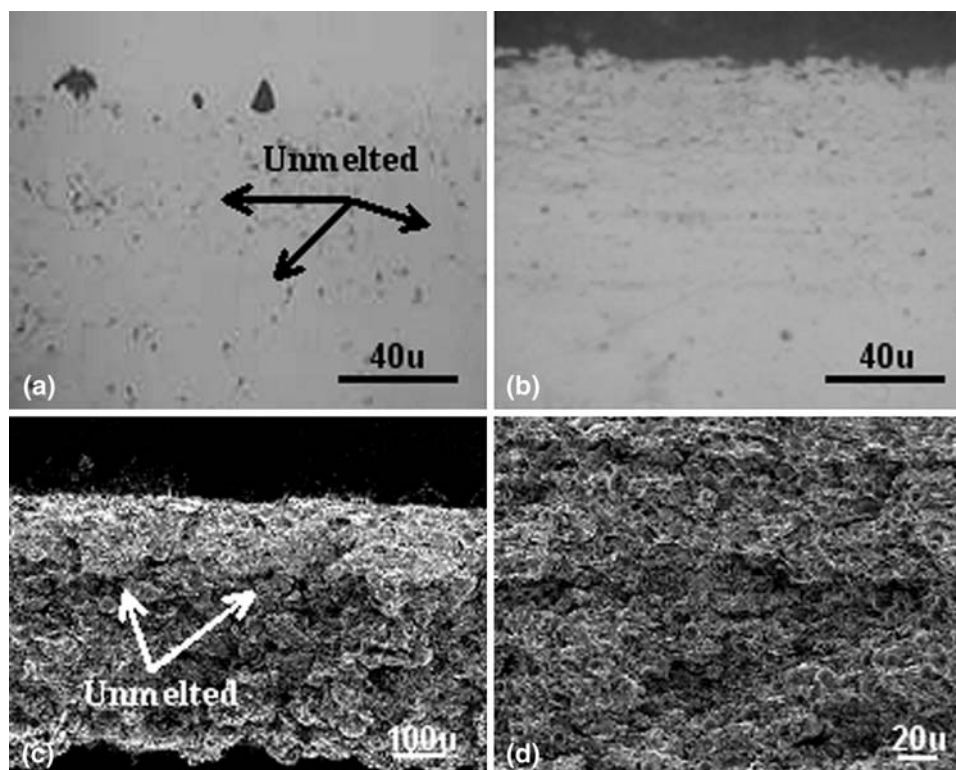


Fig. 2 Cross-sectional views of HVOF coating (a, c) and LS-HVOF (b, d). *Top row*: optical micrographs. *Bottom row*: SEM fractured morphologies

Table 1 Results of oxygen content analysis

Coatings	Oxygen contain, wt.%
Powder 1 (normal cut)	0.06
HVOF coating	1.02
LS-HVOF coating	0.287

solvent and additive has provided a protective environment to reduce oxygen partial pressure in the process.

The grain structure and oxide phase formation have been investigated using TEM analyses. From Fig. 3, it is verified that HVOF coating consists of dominantly large grains ($>1 \mu\text{m}$). It is assumed that the large grains correspond to those unmelted or partially melted particles. The higher magnification TEM indicates the presence of nanosized grains within the melted splats (Fig. 3b). Some of the dark phases are identified as oxides by diffraction analyses. The potential oxides include Cr_2O_3 , SiO_2 , and/or $(\text{Ni,Cr,Si})_x\text{O}_y$, with average grain sizes of 50-100 nm. As to the LS-HVOF coating shown in Fig. 3(c) and (d), the coating consists of dominant nanosized grains ($<100 \text{ nm}$) and some ultrafine grains ($<0.2 \mu\text{m}$), but no large grains ($>1 \mu\text{m}$). It is believed that the formation of the nanograins and ultrafine grains is associated with the melting of the particles and the rapid quenching of the melted droplets on the substrate. The oxides were surely formed during HVOF process, but oxide contents were not measured by TEM analyses. By comparing the grain

difference in the two coatings, it is further thought that a higher degree of melting and a higher quenching rate can be easily achieved for small size droplets than for large size droplets. Consequently, a high percentage of nanograins are obtained in the LS-HVOF coating. The results indicate that nanograined coatings can be cost-effectively produced from small particles without having to use expensive nanoparticles.

3.2 Physical Property

Vickers microhardness HVN (load: 300 g) was measured. The hardness value is about 530 ± 41 for HVOF-formed coating and about 620 ± 32 for LS-HVOF-formed coating. The increase in hardness in LS-HVOF coating should be related to the increased cohesive strength among the well-melted and bonded splats as well as the increase in coating density.

To confirm the above result of increased hardness in the nanograined LS-HVOF coating compared to the coarse-grained HVOF coating, nanohardness was measured on both the coatings using a nano-indentation technique, and exemplary results for the LS-HVOF coating are shown in Fig. 4. The modulus and hardness were estimated from the load-displacement curves in Fig. 4(a), and their changes as a function of displacement are given in Fig. 4(b) and (c), respectively. For the results of modulus, LS-HVOF coating is about 131 GPa, much higher than HVOF coating of about 85 GPa. For the results of

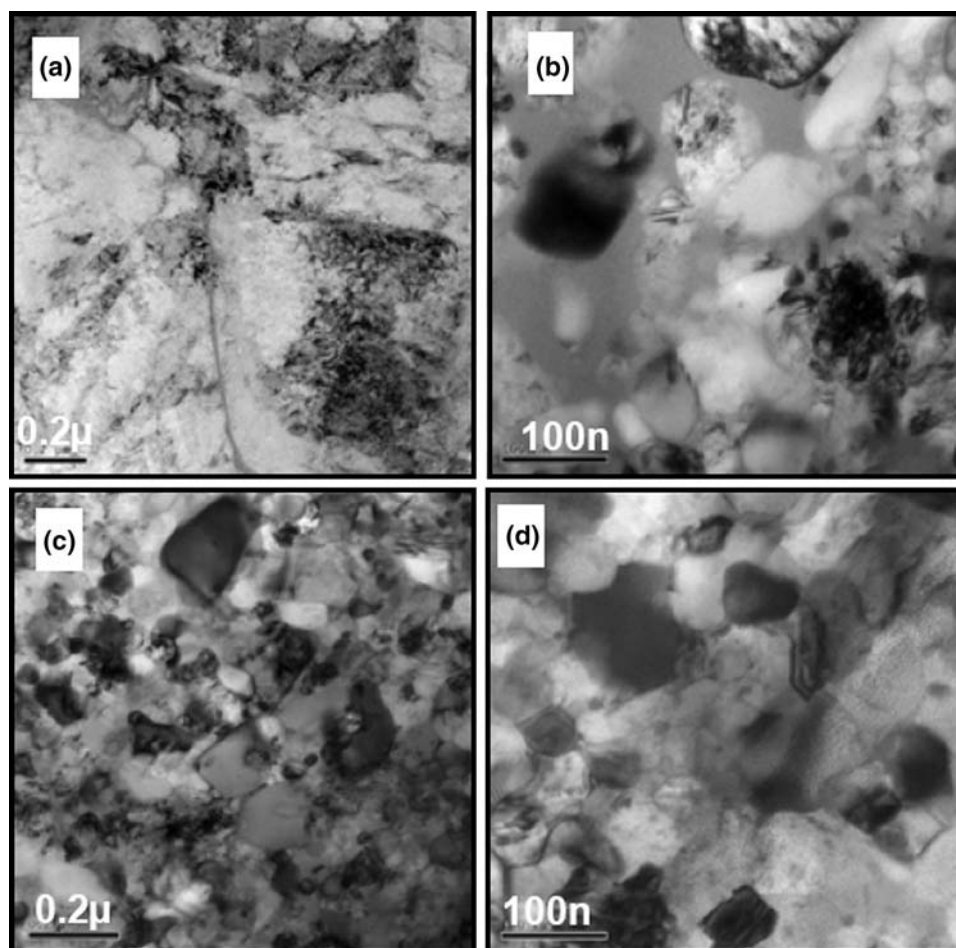


Fig. 3 TEM analyses on the grain sizes and oxide phases in the coatings of (a, b) HVOF coating and (c, d) LS-HVOF coating

nanohardness, LS-HVOF coating is about 7.2 GPa, much higher than HVOF coating of about 5.6 GPa. Therefore, the LS-HVOF coating has higher modulus and hardness than its HVOF counterpart. The results of nanohardness are consistent with those of microhardness. As to the comparison between nano- and microhardness, nanohardness value is about 31% higher than microhardness for the LS-HVOF coating and 8% higher for the HVOF coating. Other studies have shown similar results: nano-indentation hardness is about 10-30% larger than the microhardness for copper, stainless steel, and nickel titanium (Ref 7). It is assumed that the increases in modulus and hardness are attributed to the formation of high percentage of nanograins in the LS-HVOF coating.

3.3 Mechanical Behavior

For coatings in engineering applications, their mechanical behavior under loading and/or strain is of vital importance. As indicated in Fig. 5, the coatings made by HVOF and LS-HVOF processes have been tested under tensile and compressive strain in 90°- and 180°-bend tests, respectively. The results of coating inspection after the

tests show obvious difference in coating damages among the coating samples.

3.3.1 Type 1: 90°-tensile Bend Test. HVOF NiCrBSi coating (A1) has one big crack starting on the bending tip (smallest radius), and propagating laterally along the coating/substrate interface to cause a delamination. LS-HVOF NiCrBSi coating (B1) has no major damage, except a few cracks in the edge area.

3.3.2 Type 2: 90°-compressive Bend Test. Under a compressive strain, no visible damage is observed in either HVOF (A2) or LS-HVOF NiCrBSi coating (B2), except a few cracks.

3.3.3 Type 3: 180°-tensile Bend Test. In general, the coating samples suffered less damage in 180°-bend tests than in 90°-bend tests, and again the damages induced in LS-HVOF coating is less severe than those in HVOF coating. HVOF coating (A3) cracked evenly, but was still attached to the substrate. LS-HVOF coating (B3) indicated good integrity without visible cracking or spalling. In summary, the results indicate that the LS-HVOF sprayed coating is more flexible/ductile and strongly adherent under a tensile or compressive strain. The improved strain compliance in the LS-HVOF coating should be attributed

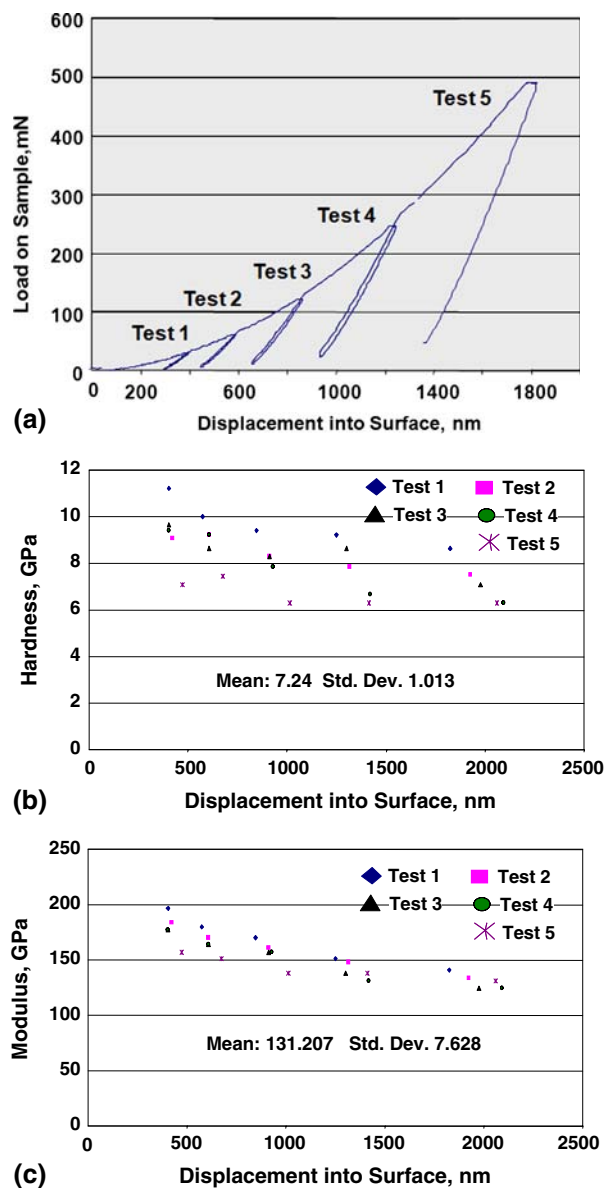


Fig. 4 Nanoindentation test in (a) LS-HVOF NiCrBSi coating and (b, c) the results of estimated hardness and modulus in the coating, respectively

to an increase in coating ductility, adhesion, cohesion, and a high degree of melting of the small particle feedstock in the LS-HVOF process.

Progressive load scratch test was conducted to test coating ductility and adhesion. A typical load-depth curve is illustrated for a HVOF coating in Fig. 6. It is noticed that there are two major coating cracking events observed under optical microscope during the progress of loading. The two critical failure points correspond to the first cracking within the coating starting at about 84 N and the second cracking at the coating/substrate interface at about 100 N. The scratched areas formed on the surface of the tested coatings are indicated as white streaks in Fig. 6(a) and (b). The Fig. 6(a) shows the semicircular cracks induced at the second critical load and the indenter has

nearly reached the substrate. The Fig. 6(b) shows the case of no cracking in LS-HVOF coating, indicating a smooth transition from the coating to the substrate at 90 N. No cracking suggests a high ductility and a strong adhesion of the coating with its substrate. Although more data need to be collected for statistic analysis, the tests have indicated that this PLST method provides a powerful tool to determine coating mechanical properties in a quantitative manner.

3.4 Oxidation Behavior

The early-stage oxidation kinetics of the coatings was measured by TGA analyses at 800 °C in air. In Fig. 7(a), the curves of oxidation kinetics indicate that both coatings obey nearly the parabolic law for weight gaining, but LS-HVOF NiCrBSi coating gained weight earlier and faster than its HVOF counterpart. After the early stage of rapid growth (150-200 min), the oxidation of LS-HVOF coating reaches a stable stage at lower rates for thermally grown oxide (TGO) growth. Alloy materials can form a protective oxide scale based on selective oxidation of elements such as Al, Cr, and Si. The rapidly formed oxide scale will provide better protection of the base alloy. Many studies have confirmed that ultrafine/nanograined alloys or coatings can promote selective oxidation of active elements and thus enhance oxidation resistance (Ref 8, 9). Therefore, the TGA test verified that LS-HVOF coating with nanometer grains is advantageous to provide superior oxidation resistance by promoting early and fast formation of protective oxide scale. At this moment, however, there is no data to support the formation of pure oxide scale such as α -alumina.

Long-term oxidation tests were conducted at 800 °C for 500 h in air. The weight gains seem to obey the parabolic law, and the parabolic constants K_p were estimated for the coatings tested by curve fitting the weight gain-time curves shown in Fig. 7(b). The K_p values are $16.9 \times 10^{-7} \text{ mg}^2/\text{mm}^4 \text{ hr}$ for the HVOF coating and $0.2 \times 10^{-7} \text{ mg}^2/\text{mm}^4 \text{ hr}$ for the LS-HVOF coating, respectively. Obviously, the LS-HVOF coating exhibits much lower long-term TGO rate than its HVOF counterpart. Based on the microstructures observed on the two coatings, it can be concluded that the microstructural features such as density grain size and defect inclusions (unmelts, etc.) play a determinable role on the oxidation behavior of the coatings having identical chemical composition. The lower K_p value with LS-HVOF coating should be greatly attributed to the formation of well-melted finer grained and bonded splat structure in the coating as well as improved coating density and uniformity.

3.5 Hot Corrosion Test

Accelerated hot corrosion tests were performed by prepainting of the coating samples with a mixture of $\text{Na}_2\text{SO}_4 + 20\% \text{NaCl}$ salts, and then tested at 800 °C in air. Figure 8 shows the kinetic behavior of the coatings tested in the salt mixture. Firstly, all the coatings keep losing weight during the test period, indicating the coatings were chemically attacked without forming complete protective





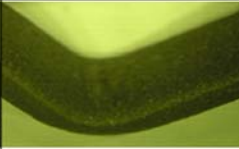

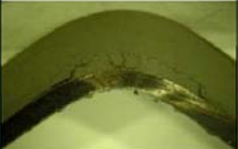

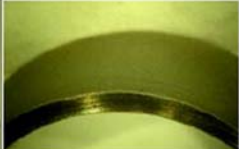
Coatings	Bend Tests (90°)		Bend Test (180°)
	Type1: Tensile	Type2: Compressive	Type 3: Tensile
Schematic			
HVOF Coating			
	A1. Crack & Peel	A2. No major crack	A3. Many cracks
LS-HVOF Coating			
	B1. Edge crack only	B2. No major damage	B3. No visible crack

Fig. 5 Macrographs of the coatings after tested in 90°- and 180°-bending tests

oxide scales in the salt mixture. Secondly, LS-HVOF coating seems to be more resistant to this corrosion environment with much less weight loss relative to its HVOF coating counterpart.

The tested coatings were observed on the cross-sectional microstructures, which are shown in Fig. 9. In the HVOF coating (9a), corrosion took place severely in near surface zone and penetrated deeply down to the coating/substrate interface. In the LS-HVOF NiCrBSi coating (9b), the coating was corroded only in the near surface zone, without corrosion penetration deeply into the interface of coating and substrate. Therefore, if the corrosion resistance is measured by the depth of corrosion, undoubtedly, the LS-HVOF coating is more resistant to the hot corrosion than the HVOF coating counterpart. XRD analyses were used to determine the composition of the corroded surface layers. The main phases identified on the corroded surface include SiO_2 , Cr_2O_3 , Fe_2O_3 , and minor FeS or Fe_7S_8 .

Many investigations have revealed that the presence of sulfur in the form of sulfates can cause internal sulfidation of alloys beneath the external oxide layer. The addition of chlorides can cause the formation of volatile species, which form voids and pits at grain boundaries, thus forming an easy path for flow of corrosives (Ref 10). The studies on HVOF-sprayed Ni-Cr-W-Mo-B coatings (NiCrWMoB, NiCr, NiCrMo, etc.) found that the corrosion resistance of the HVOF alloy coatings can be improved by heat treatment due to increased microstructural and chemical homogeneity, such as the reduction of porosity and densification (Ref 11). The studies on laser remelting of HVOF coatings reported that the treated coatings suffered

much less corrosion damage, whereas as-sprayed coating was penetrated by corrosive species. Laser remelting efficiently removed the interconnected network of voids and oxides at splat boundaries of the HVOF coatings (Ref 12). Therefore, it can be concluded that the corrosion resistance of the LS-HVOF coating has been improved by the formation of well-bonded splats at their boundaries and less porosity structure due to well-melting of the small particles used in LS-HVOF spraying. As a result, the less defective and homogenous coating structure provides fewer paths for the penetration of corrosives. With the presence of the nanograins in the LS-HVOF coating, additionally, enhanced ability for selective oxidation should also contribute to the improvement, at least prolonging the transition time before hot corrosion process moves from an initiation stage to a propagation stage.

It is worthy to point out that this work has been originally performed based on the US DOE specially funded program titled as "Surface Modification of Alloys for Ultra-supercritical Coal-Fired Boilers (USC)." This program aims to seek innovative surface modification methods for a reliable and durable USC boiler system. The extensive tests above have been conducted to evaluate coating performance in simulated USC operating conditions, typically with steam temperatures up to 760 °C and pressures up to 37.9 MPa. Besides the boiler application, the process is applicable to make superior metallic coatings required in other advanced industry applications, such as a bondcoat in thermal barrier coating. The process is capable of producing a fine-structured or nanostructured coating using small-sized (a few microns and submicrons) or nanosized particles in a liquid suspension. As to coating

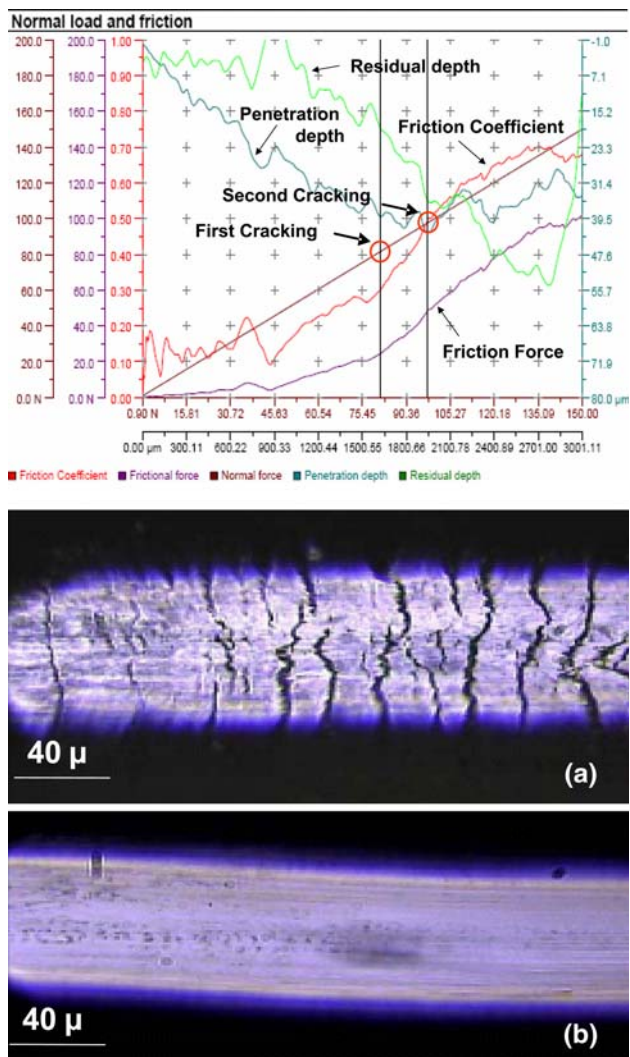


Fig. 6 A typical load-depth curve for HVOF coating tested in progressive load scratch test. Micrographs of (a) tested HVOF coating and (b) tested LS-HVOF coating

materials, so far more than five types of alloy coatings including Inconel 625 have been produced by LS-HVOF spray.

4. Conclusions

An innovative LS-HVOF process has been developed to realize ultrafine-grained alloy coating deposition by utilizing liquid suspension containing small metallic particles. Experimental investigations have been conducted to compare physical and mechanical properties, oxidation resistance, and hot corrosion behaviors of the coatings produced by conventional HVOF and innovative LS-HVOF processes. Results have shown that LS-HVOF NiCrBSi coating has superior properties and performance in comparison with its HVOF counterpart: (i) Microstructure evaluation verified that a nanograined

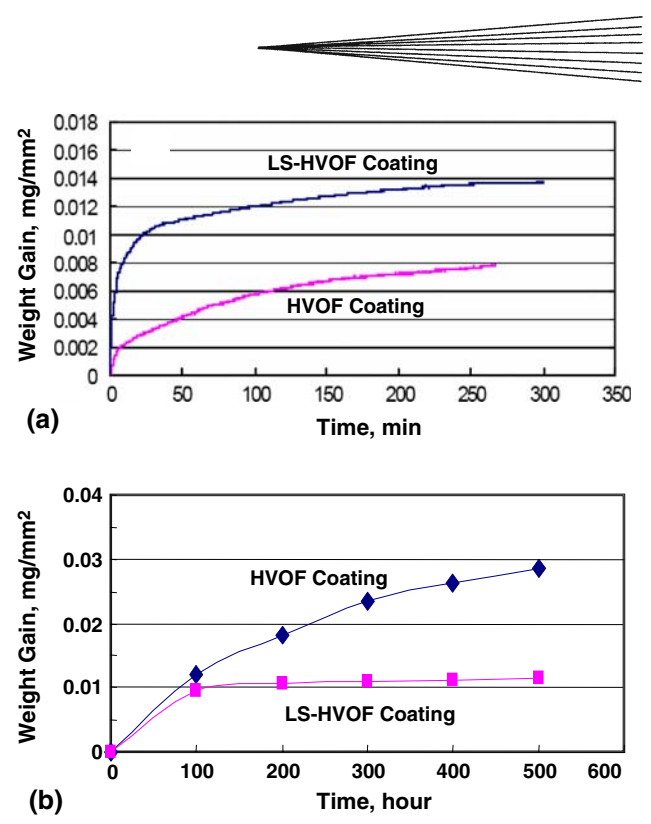


Fig. 7 Curves of isothermal oxidation kinetics. (a) Short-term TGA tests at 800 °C in air and (b) Long-term furnace tests at 800 °C in air

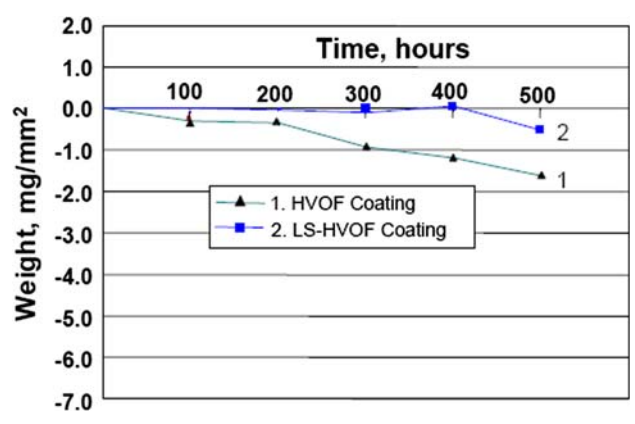


Fig. 8 Kinetic behaviors of hot corrosion for the coatings tested in the mixture of Na₂SO₄ + 20wt.% NaCl salts at 800 °C in air

microstructure is produced in the LS-HVOF coating with high percentage of melted splats, low defects, and good uniformity; (ii) physical property results indicated that the nanostructured coating has a relative higher hardness and modulus; (iii) mechanical property tests clarified that LS-HVOF coatings have higher ductility and cohesive and adhesive strength and maintain good coating integrity with higher strain resistance when tested under a tensile or compressive load; (iv) oxidation tests indicated that nanostructured LS-HVOF coating can form a protective oxide scale rapidly in the early stage of oxidation and has a lower TGO growth rate for long-term exposure at 800 °C;

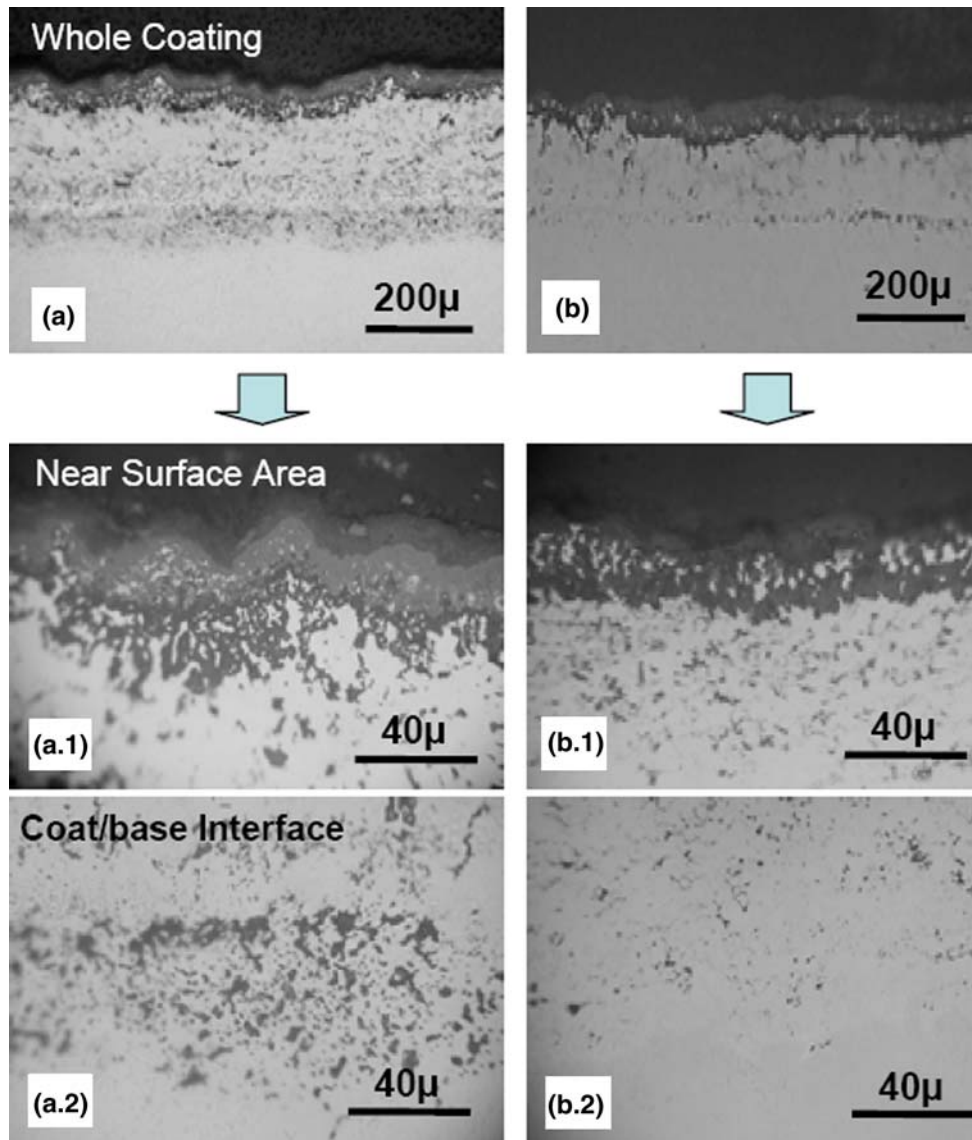


Fig. 9 Microstructures of the coatings tested in the mixture of $\text{Na}_2\text{SO}_4 + 20\text{wt.}\% \text{NaCl}$ salts at 800°C for 500 h. (a) HVOF coating and (b) LS-HVOF coating

and (v) hot corrosion tests revealed that the LS-HVOF coating is more resistant to hot corrosion in $\text{Na}_2\text{SO}_4 + 20\text{ wt.}\% \text{NaCl}$ at 800°C than its HVOF counterpart. The main contributors to these improvements include higher degree of melting and higher velocity of the small particles. Therefore, LS-HVOF technique is very promising for making superior coatings in many advanced industry applications such as ultrasupercritical boiler components.

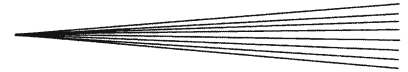
Acknowledgments

The authors thank Mr. Jeff Roth at Inframat Corporation for his assistance in conducting HVOF spray trials. This work was supported by US Department of

Energy (Grant No. DE-FG02-06ER-84604) managed by Mr. U. Rao and Ms. P. A. Rawls.

References

1. X. Ma, F. Wu, J. Roth, M. Gell, and E.H. Jordan, Low Thermal Conductivity Thermal Barrier Coating Deposited by the Solution Plasma Spray Process, *Surf. Coat. Technol.*, 2006, **201**(7), p 4447-4452
2. M. Gell, E.H. Jordan, M. Teicholz, B.M. Cetegen, N. Padture, L. Xie, D. Chen, X. Ma, and J. Roth, Thermal Barrier Coatings Made by the Solution Precursor Plasma Spray Process, *J. Therm. Spray Technol.*, 2008, **17**(1), p 1-12
3. P. Fauchais, Understanding Plasma Spraying, *J. Phys. D: Appl. Phys.*, 2004, **27**, p R86-R108
4. X. Ma, J. Roth, D.W. Gandy, and G.J. Frederick, A New High-velocity Oxygen Fuel Process for Making Finely Structured and



- Highly Bonded Inconel Alloy Layers from Liquid Feedstock, *J. Therm. Spray Technol.*, 2006, **15**, p 670-675
5. M. Gaona, R.S. Lima, and B.R. Marple, Nanostructured Titania/Hydroxyapatite Composite Coatings Deposited by High Velocity Oxy-fuel (HVOF) Spraying, *Mater. Sci. Eng. A*, 2007, **458**, p 141-149
 6. A. Killinger, M. Kuhn, and R. Gadow, High-velocity Suspension Flame Spraying (HVSFS), a New Approach for Spraying Nanoparticles with Hypersonic Speed, *Surf. Coat. Technol.*, 2006, **201**, p 1922-1929
 7. L.M. Qian, et al., Comparison of Nano-indentation Hardness to Microhardness, *Surf. Coat. Technol.*, 2005, **195**, p 264-271
 8. F. Liu, W. Gao, K. Dahm, and F. Wang, The Effect of Coating Grain Size on the Selective Oxidation Behavior of Ni-Cr-Al Alloy, *Scripta Mater.*, 1997, **37**(10), p 1551-1558
 9. G. Chen and H. Lou, Effect of Nanocrystallization on the Oxidation Behavior of a Ni-8Cr-3.5Al Alloy, *Oxid. Met.*, 2000, **54**, p 155-162
 10. D. Deb, S.R. Lyster, and V.M. Radhakrishnan, A Comparative Study of Oxidation and Hot Corrosion of a Cast Nickel Base Superalloy in Different Corrosive Environments, *Mater. Lett.*, 1996, **29**, p 19-23
 11. C.H. Lee and K.O. Min, Effects of Heat Treatment on the Microstructure and Properties of HVOF-sprayed Ni-Cr-W-Mo-B Alloy Coatings, *Surf. Coat. Technol.*, 2000, **132**, p 49-57
 12. M.A. Uusitalo, P.M.J. Vuoristo, and T.A. Mantula, High Temperature Corrosion of Coatings and Boiler Steels in Reducing Chlorine-containing Atmosphere, *Surf. Coat. Technol.*, 2002, **161**, p 275-285